Journal of Nuclear Materials 386–388 (2009) 520–524

Contents lists available at ScienceDirect

Journal of Nuclear Materials

journal homepage: www.elsevier.com/locate/jnucmat

High-temperature strength analysis of welded joint of RAFs by small punch test

Taichiro Kato [a], Shin-ichi Komazaki [a,*], Yutaka Kohno [a], Hiroyasu Tanigawa [b], Akira Kohyama [c]

[a] Department of Materials Science and Engineering, Muroran Institute of Technology, Muroran 050-8585, Japan
[b] Naka Fusion Institute, Japan Atomic Energy Agency, Tokai 319-1195, Japan
[c] Institute of Advanced Energy, Kyoto University, Uji 611-0011, Japan

A B S T R A C T

Type IV creep damage has recently been a worldwide issue for high Cr ferritic steels. The small punch (SP) creep test has been successfully applied to evaluate this damage of low alloy ferritic steel by the author's group. However, the heat affected zone (HAZ) of fusion reactor material welded by electron-beam (EB) welding is so thin that it is not easy to evaluate its mechanical properties by the conventional SP test. In this study, the SP test using a further miniaturized specimen was applied to the EB welded joint of reduced activation ferritic steel (RAFs), for evaluating high-temperature tensile properties of the HAZs. As the result, the σ_y and σ_B of the tempered HAZ at 873 K were estimated to be as low as 275–300 MPa and 325–340 MPa, respectively.

1. Introduction

Reduced activation ferritic steels (RAFs), *e.g.*, F82H (8Cr–2W–VTa) and JLF-1 (9Cr–2W–VTaN), are candidate materials for the Japanese ITER test blanket module (TBM) [1]. The blanket systems are very complex and have many integrated functions, materials and interfaces. They consist of several parts such as first wall, side and back plates, feeding and coolant pipes and so on [2]. Therefore welding process like an electron-beam (EB) welding is essential for fabricating the blanket [3].

On the other hand, premature failures at the welded joint have recently been a worldwide issue in 9–12% chromium ferritic steels [4,5]. The failure occurs at the outer edge of heat affected zone (HAZ), *i.e.*, the fine grain HAZ (FGHAZ) and it is known as 'Type IV creep damage'. Komazaki et al. [6] successfully applied the small punch (SP) creep test to the creep property evaluation of the HAZ of the boiler header. However, the HAZ formed by EB welding is so thin that it is not easy to evaluate the mechanical properties of such local and limited region by the conventional SP test. It is known that the specimen thickness and/or the number of grains included in the thickness have an influence on the observed mechanical properties for thin sheet-type tensile specimens [7]. Toloczko et al. [8] investigated the effects of specimen thickness (t) and the ratio of the specimen thickness to the grain size (t/d_g) on the mechanical properties of 316 stainless steel by the shear punch test which is very similar to the SP test. It was revealed from their results that there was no significant effect of either t or t/d_g on the shear strengths and the ductility and the shear punch test was not as sensitive to t or t/d_g as was the tensile test. This reduced sensitivity to specimen thickness seems to permit the SP creep test using a further miniaturized specimen.

In this study, the SP test with a constant deflection rate was carried out at the temperatures of 673–873 K by using a TEM disk-type specimen (ϕ 3.0 × 0.25 mm), preliminary to the SP creep test. The test was applied to the coarsen grain HAZ (CGHAZ), FGHAZ and tempered HAZ (THAZ) samples removed from the EB welded joint of the RAFs, F82H IEA heat. The high-temperature tensile properties of those HAZs were estimated based on the correlations between the results obtained from the SP test and the tensile test of the base metal.

2. Experimental procedures

2.1. Materials

The RAFs, F82H IEA heat, was used in this study. The chemical composition and heat treatment condition of the hot rolled plate, 15 mm in thickness, are given in Table 1. The plates with I-grove were welded by the EB welding. A welding speed of 400 mm/min was achieved with an electron beam of 0.2 A and 90 kV. Subsequently, the welded joint was subjected to the post weld heat treatment of 993 K/1 h.

2.2. Small punch tests

A rod-type samples, 3 mm in diameter and 55 mm in length, was taken perpendicular to the fusion line by a wire-cut electric discharge machining (EDM), schematically illustrated in Fig. 1. Next, a disk specimen, 0.35 mm in thickness, was sliced off from

* Corresponding author. Tel.: +81 143 46 5668; fax: +81 143 46 5601.
E-mail address: komazaki@mmm.muroran-it.ac.jp (S. Komazaki).

0022-3115/$ - see front matter © 2009 Elsevier B.V. All rights reserved.
doi:10.1016/j.jnucmat.2008.12.153

Table 1
Chemical composition (wt.%) and heat treatment condition of F82H IEA heat.

	Cr	W	V	Ta	C	B	Mn	N	Fe
Base metal	7.71	1.95	0.16	0.02	0.09	0.0002	0.16	0.006	Bal.

1313 K × 38 min (normalizing) + 1023 K × 60 min (tempering).

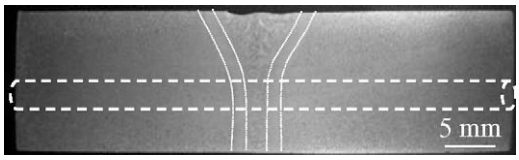

Fig. 1. Cross-sectional view of EB welded joint.

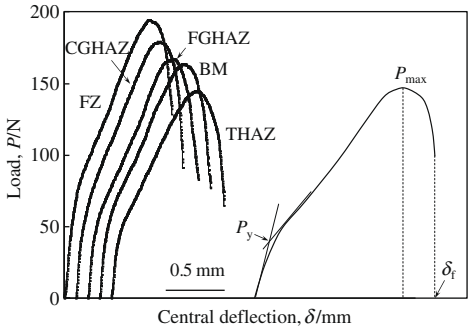

Fig. 4. Load-central deflection curves measured at 873 K and definitions of P_y, P_{max} and δ_f.

the CGHAZ, FGHAZ, THAZ, base metal (BM) and fusion zone (FZ) by the EDM. Each local region was determined based on the below-mentioned results of microstructure observation and Vickers hardness test. Both the specimen surfaces were grinded and mechanically polished up to 0.05 μm alumina powder finish and the specimen's thickness was finally adjusted to 0.25 ± 0.005 mm.

The SP tests were performed at the temperatures ranging from 673 to 873 K in addition to room temperature (293 K). A load was applied to the center of the specimen through the Si_3N_4 ball, 1.0 mm in diameter, using the electric servo motor. The deflection rate was fixed at 0.2 mm/min. All the tests were carried out in an argon gas atmosphere and the gas was continuously passed through during the test to prevent severe oxidation of the specimen. Additionally, a titanium wire mesh was placed near the specimen holder to take residual oxygen away from the atmosphere.

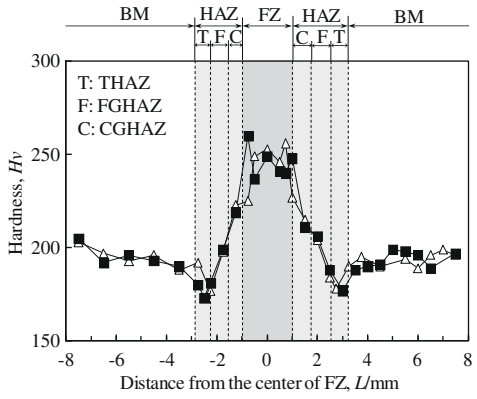

Fig. 2. Hardness distribution of EB welded joint.

3. Results and discussion

3.1. Hardness and microstructure

Fig. 2 shows the Vickers hardness distribution measured perpendicular to the fusion line at room temperature. It is worthy of note that the HAZ's hardness is as low as 175 Hv, which is lower than the BM's one, at around the HAZ/BM interface, namely, the THAZ. In the THAZ where the temperature does not exceed A_{c1} during the welding, the welding heat merely tempers the existing martensite and causes the softening.

Fig. 3 shows the optical and scanning electron micrographs of the FZ, CGHAZ, FGHAZ, THAZ and BM. All the samples exhibited a typical martensitic structure, although the prior austenite grain size showed a slight difference. However, the precipitate size of the THAZ was observed to be slightly larger than those of the others and its block grains were more equiaxed.

3.2. Small punch test results of HAZs

Fig. 4 shows the load versus central deflection curves measured at 873 K. The overall shape and general futures of the curve are in good agreement with the curve measured by using the conventional specimen ($10 \times 10 \times 0.5\ mm^3$) [9]. As shown in Fig. 5, all of the fractures occurred along the circumference where the equivalent stress and/or strain were largest. The fracture mode showed

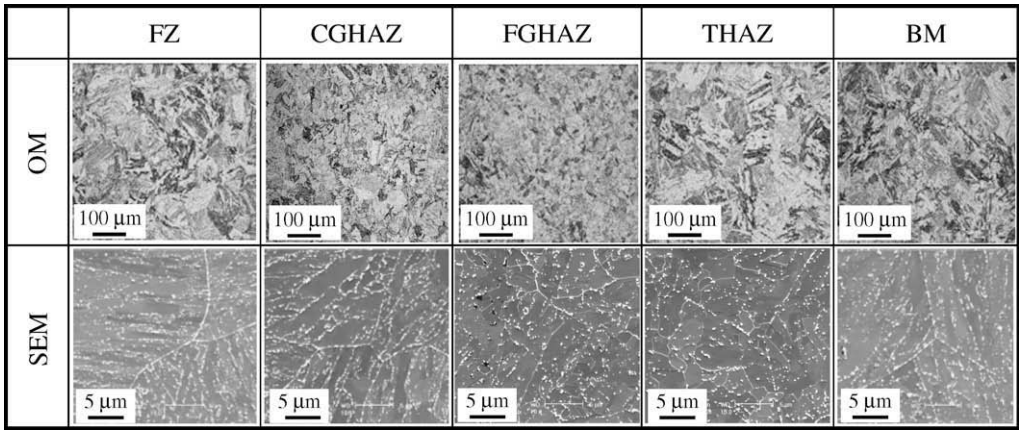

Fig. 3. OM and SEM micrographs of FZ, CGHAZ, FGHAZ, THAZ and BM.

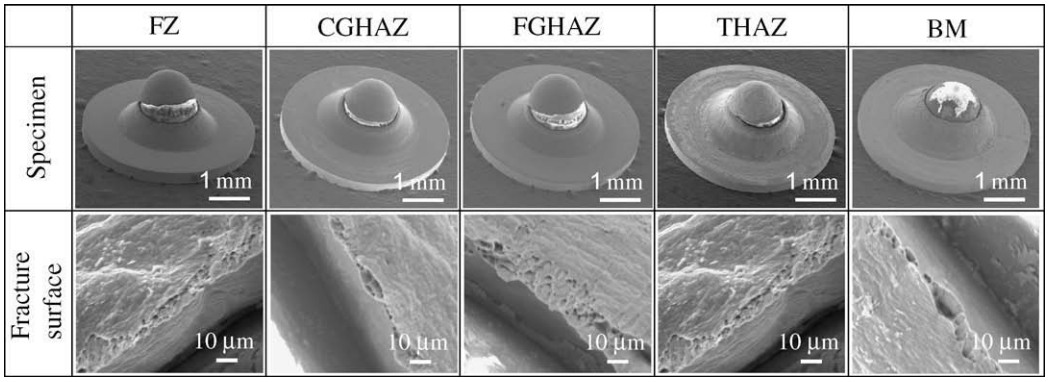

Fig. 5. SEM micrographs of FZ, CGHAZ, FGHAZ, THAZ and BM specimens tested at 873 K.

no significant change and all the specimens exhibited a typical ductile fracture surface.

It has been reported that the load at the initial localized plastic straining denoted by P_y (Fig. 4) and the maximum load, P_{max}, are closely associated with the yield strength, σ_y, and the ultimate tensile strength, σ_B, respectively [10]. Fig. 6 shows the P_y and P_{max} determined in the welded joint, as well as the fracture deflection, δ_f, which corresponds to the total elongation (*TE*). The variation in the P_{max} is very similar to that in Vickers hardness (Fig. 2). In the HAZ, it is inclined to decrease from the FZ to the BM and it reaches a certain minimum value at the THAZ. A similar trend can be also seen in the change in the P_y. These reductions in strength at the THAZ are likely to be attributable to the above-mentioned recovery of microstructure caused by overtempering. Contrary to the P_y and P_{max}, the δ_f decreases with approaching the FZ from the BM, and the ductility of the FZ is relatively low.

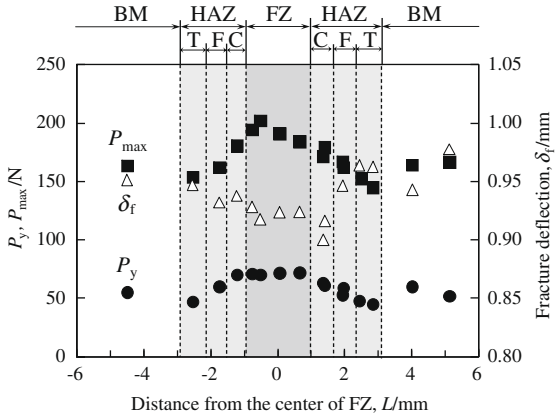

Fig. 6. Distributions of P_y, P_{max} and δ_f measured at 873 K.

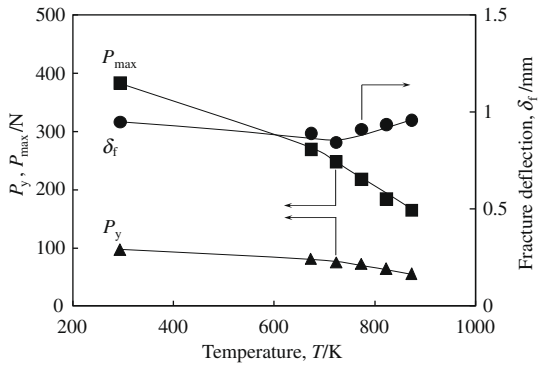

Fig. 7. Temperature dependences of P_y, P_{max} and δ_f measured on the BM.

3.3. High-temperature tensile properties of HAZs

The P_y, P_{max} and δ_f measured on the BM are plotted as a function of testing temperature in Fig. 7. The P_y and P_{max} decrease monotonously with increasing temperature, and these variations agree with those in the σ_y and σ_B, respectively (Fig. 8 [11]). The temperature dependence of δ_f is different from that of the P_y or P_{max}. It tends to decrease slightly until 723 K, but, after that, it increases gradually with increasing temperature to the contrary. However, this temperature dependence is also qualitatively identical to that of the *TE* (Fig. 8 [11]). Fig. 9 shows the correlations between the σ_y, σ_B and *TE* and the P_y, P_{max} and δ_f, respectively. There are almost linear correlations between them, although some scattering results can be seen in the relationship between the *TE* and the δ_f. The quantitative correlations were determined by the method of least squares, resulting in the below equations,

$$\sigma_y = 4.8P_y + 61 \quad (1)$$

$$\sigma_B = 1.3P_{max} + 137 \quad (2)$$

$$TE = 51.5\delta_f - 28 \quad (3)$$

Fig. 10 shows the distributions of the σ_y, σ_B and *TE* at 873 K, which were estimated by Eqs. (1)–(3), respectively. It is apparent from Fig. 10(a) and (b) that the THAZ has the lowest strength whereas the FZ the highest one. The σ_y and σ_B of the THAZ are around 275–300 MPa and 325–340 MPa, respectively. Correspondingly, the *TE* of the FZ and the CGHAZ are lower than that of the BM.

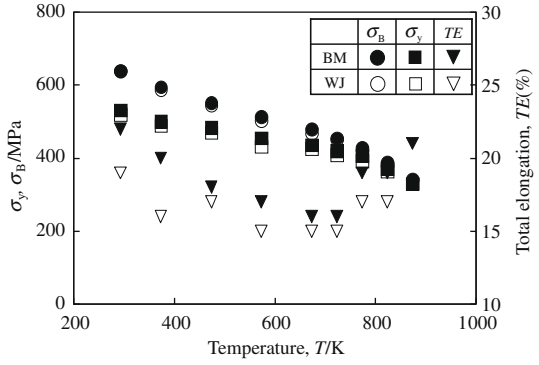

Fig. 8. Temperature dependences of σ_y, σ_B and *TE* of the base metal (BM) and EB welded joint (WJ) [11].

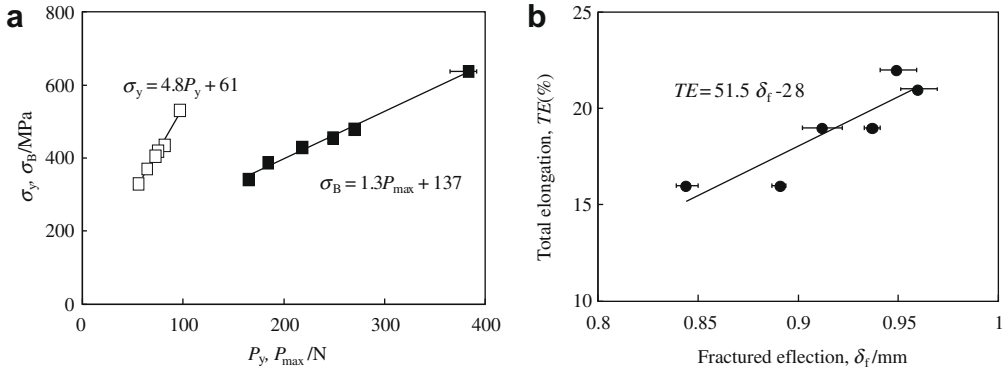

Fig. 9. Relationship between the results of SP test and uniaxial tensile test. (a) $\sigma_y - P_y$, $\sigma_B - P_{max}$. (b) $TE - \delta_f$.

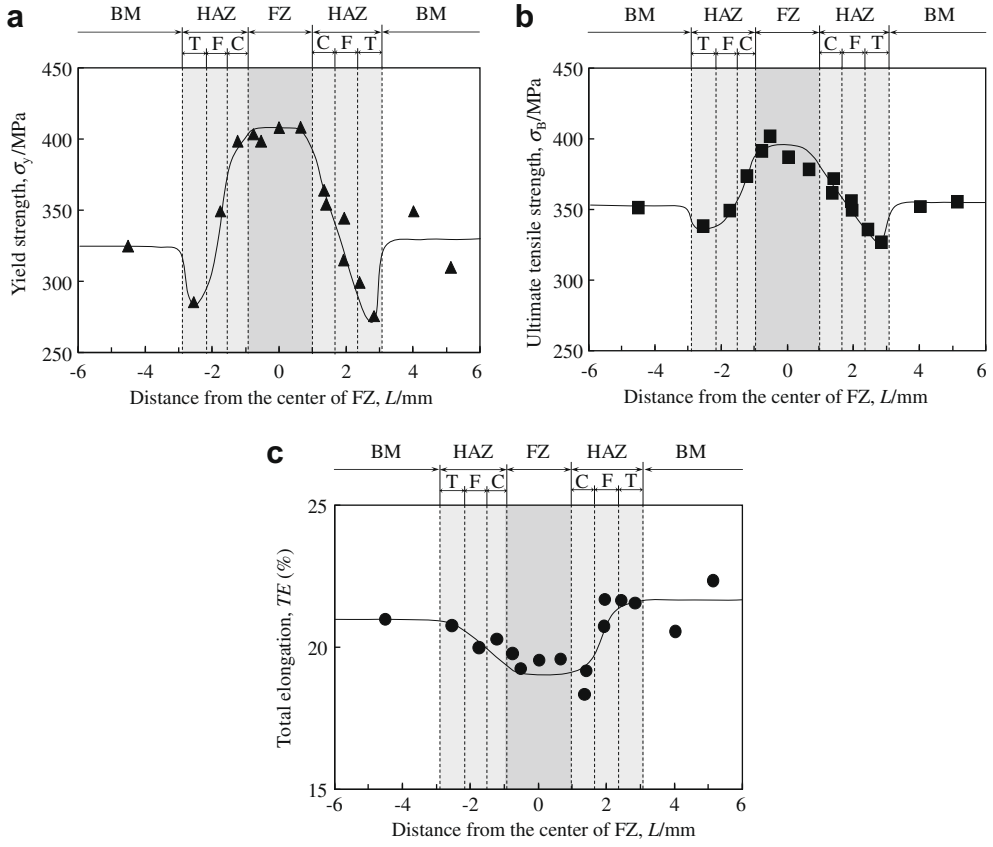

Fig. 10. Distributions of tensile properties estimated by Eqs. (1)–(3). (a) σ_y. (b) σ_B. (c) TE.

However, as can be clearly seen in Fig. 8, there are no such large differences between the σ_y and σ_B of the welded joint (WJ) specimen including the softened THAZ and those of the BM specimen. This discrepancy between two results seems to result from the plastic constraint of the thin THAZ. It can be also seen from Fig. 8 that the TE of the WJ specimen is smaller than that of the BM one. This result is caused by the difference in ductility between the FZ and the BM (Fig. 10(c)), namely, the decrease in gauge length of the more ductile BM in the WJ specimen. Consequently, the SP test using a TEM disk-type specimen is expected to be strong tool for estimating the high-temperature tensile properties of local HAZ regions, although more tests for more samples are needed for increasing the reliability of experimental data.

4. Conclusions

The SP test using a TEM disk-type specimen (ϕ 3.0 × 0.25 mm) was applied to the CGHAZ, FGHAZ and THAZ samples removed from the EB welded joint of F82H IEA heat. The high-temperature tensile properties of the HAZs were estimated based on the correlations between the results obtained from the SP test and the tensile test of the base metal. The experimental results reveal that there are almost linear correlations between the σ_y, σ_B and total elongation (TE) and the P_y, P_{max} and δ_f, respectively. From these correlations, it is found that the σ_y and σ_B of the THAZ at 873 K are as low as 275–300 MPa and 325–340 MPa, respectively, and the ductility of the FZ is relatively low.

References

[1] A. Kohyama, Mater. Trans. 46 (2005) 384.
[2] M. Enoeda, M. Akiba, S. Tanaka, A. Shimizu, A. Hasegawa, S. Konishi, A. Kimura, A. Kohyama, A. Sagara, T. Muroga, Fus. Eng. Des. 81 (2006) 415.
[3] K. Shiba, M. Enoeda, S. Jitsukawa, J. Nucl. Mater. 329–333 (2004) 243.
[4] Y. Hasegawa, T. Muraki, M. Ohgami, Tetsu-to-Hagané 90 (2004) 609.
[5] Y. Hasegawa, T. Muraki, M. Ohgami, Tetsu-to-Hagané 92 (2006) 618.
[6] S. Komazaki, T. Sugimoto, Y. Hasegawa, Y. Kohno, ISIJ Int. 47 (2007) 1228.
[7] S. Miyazaki, K. Shibata, H. Fujita, Acta Metall. 27 (1979) 855.
[8] M.B. Toloczko, Y. Yokokura, K. Abe, M.L. Hamilton, F.A. Garner, R.J. Kurtz, Small Specimen Test Techniques, Fourth Volume, in: M.A. Sokolov, J.D. Landes, G.E. Lucas (Eds.), ASTM STP, vol. 1418, ASTM International, West Conshohocken, PA, 2002, p. 371.
[9] T. Nakata, S. Komazaki, M. Nakajima, Y. Kohno, H. Tanigawa, K. Shiba, A. Kohyama, J. Japan, Inst. Met. 70 (2006) 642.
[10] X. Mao, H. Takahashi, J. Nucl. Mater. 150 (1987) 42.
[11] K. Shiba, Summary Report of Iea Round-Robin Testing on F82h Iea Heats in Japan, pp. D4&D5.